Universiteit Utrecht

Graduate School of Natural Sciences

Diffusion and diffusion-like effects of energy in lanthanide-doped nanocrystals

Master Thesis

René Moesbergen

Supervisors:

Sander Vonk MSc.
Dr. Laura Filion
Dr. Freddy Rabouw
Debye Institute for Nanomaterial Science

1st April 2022

Abstract

For quite some time, people have tried to fundamentally understand the processes in lanthanide-doped nanocrystals (NCs). In these materials, the ionic dopants absorb and emit photons, where the emitted photons have a different energy from the absorbed ones. This is possible due to energy transfer (ET) processes, where (a part of) the energy is transferred from one ion to another. And in order to understand the resulting emitted light, it is of importance to understand these microscopic processes. One of these ET processes is the transfer of all its energy to a neighbouring ion, resulting in an effective diffusion of energy.

In this thesis we study this diffusion and other diffusion-like effects in a thin film of $NaYF_4$:$Er^{3+}Yb^{3+}$ NCs, for which we used simulations, differential equations and experiments. First, we performed Monte Carlo simulations in order to connect the ET rate to an effective diffusion coefficient. From these simulations, we found that the diffusion has a transitioning point with respect to the doping concentration, at lower concentrations the diffusion is isotropic and at higher concentrations the diffusion is anisotropic.

Secondly we solved the differential equations for two- and three-level energy diagrams in both space and time in order to connect this diffusion coefficient to an experiment. Here we looked at the spatial distribution of the energy, which broadens due to the effective diffusion. Upon solving these equations, however, we found that are also other processes, that are not diffusion, that can lead to broadening and even narrowing of this energy distribution, which is possible due to non-linear behaviour.

To test these results, we performed experiments on tuned NCs, such that we can measure these effects independently. For this we used an experimental setup with a pulsed laser that allows us to measure the spatial intensity distribution of the emitted light. This intensity distribution is linearly dependant on the energy distribution and as such we can compare these experiments directly with the results of the differential equations. So first, we measured NCs, solely doped with Yb-ions, and found that there was no diffusion, but there was a broadening effect during the excitation. Next, we measured NCs solely doped with Er-ions and doped with both Er and Yb, where we saw the narrowing effect due to cross-relaxation and the broadening effect due to upconversion. Here, we were able to match all those experiments, without a diffusion term.

Contents

1 Introduction

Upconversion (UC) materials are materials that can absorb low-energy photons and emit them as high-energy photons. For this, these materials are increasingly used in for example bio-imaging, chemical sensing and thermometry.[1–4] And in order to control and tune the properties of these materials for their different purposes, there are many studies into the photo physics of these materials, which involves many possible processes[1, 2, 5–7]. Of particular interest are lanthanide-doped nanocrystals (NCs), such as $NaYF_4$:$Er^{3+}Yb^{3+}$. In this material, the ionic dopants erbium (Er) and ytterbium (Yb) can absorb photons in the infra-red (IR). These excited ions can than interact with eachother and transfer their energy from one ion to the other. This results in Er-ions that have more energy than the energy of one absorbed photon and these excited ions can emit all of that energy as a single photon with a higher energy than the absorbed photon. For this specific material, the emitted photons are primarily in the green. For these interactions to happen, however, the ions need to be close to eachother and have to be in the correct energy state. And since this can fluctuate within the NCs, it is important to have a microscopic understanding of the system.
It is known, for example, that at high doping concentrations, the photon UC to green light is less efficient than at low doping concentrations, an effect known as concentration quenching. [8] An explanation for this, is the fact that at high doping concentrations, the distances between ions is smaller, which means that the interactions are stronger. This in turn means that the energy can be transferred much faster, resulting in an effective diffusion. This diffusive behaviour can bring the excited states to the edge of the NC, where they lose their energy to the vibrational modes of the solvent molecules.
In this thesis we study this effective diffusion and to do this, we will use a combination of simulations, differential equations and experiments. In the first chapter we will discuss some theory about the energy diagram of $NaYF_4$:$Er^{3+}Yb^{3+}$ and reduce it as much as possible. Next we will discuss in more detail the relation between the effective diffusion coefficient and the microscopic properties of the material and we will also calculate it using a mean-field approach. In the two sections after that, we will make the connection between this effective diffusion coefficient and any experimental results. For this we use differential equations in both space and time for a two and three level system. To be able to find any analytical results, we will use approximations. Using this approach, we find that there are positive and negative diffusion-like effect that are not the result of the diffusion described above, but rather a result of non-linear processes.
In the next chapter, we will discuss the Monte Carlo simulation we use to further study the diffusion, then the synthesis procedure for the NCs and finally the setup to measure the spatial distribution of the emitted light. In the last chapter, we will look at the simulations of the diffusion in a perfect crystal and compare it to the mean-field theory that we calculated. And finally, we will compare the analytical results of the differential equations with experiments on the NCs, which we approximated using the two and three level energy diagrams. In these experiments, we are able to match the result to the analytical solutions and we will successfully show there are these diffusion-like effects. These effects can cause complications when trying to determine the diffusion coefficients, but these can be used as an extra tool to determine other parameters.

2 Theory

2.1 Energy diagrams

In this first section we will describe the energy level structure of the Yb- and Er-ions in the NCs. The most complete model for this is a nine-level energy model as given in figure 1. In this model, every Er-ion can be in either of the nine states and every Yb-ion can be in either an excited state or in the ground state. Depending on the state of an ion and the type and states of the neighbouring ions, they can either decay to a less energetic state, or they can interact with neighbouring ions and exchange energy with them.
All these processes can be divided into six categories. First of all, there is a radiative decay (R, the solid lines in the figure), where an excited state loses its energy under the emission of a photon and decays to the ground state. Next there is also a non-radiative decay (NR, the black dotted lines), in this process the ion loses some of its energy without emitting a photon. Instead, this energy is transferred to for example molecualar vibrations of solvent molecules [2].
The third and fourth processes are the cross-relaxation (CR, green dotted lines) and the upconversion (UC, yellow dotted lines) processes. In these processes, two neighbouring Er-ions interact and (some of the) energy is transferred from one Er-ion to the other. If this results in a larger energy separation between the two ions, it is called UC process and if it results in a smaller energy separation, it is called a CR process.
Lastly, we have the energy transfer (ET, red dotted lines) and the back-energy transfer (BET, blue dotted lines) processes. These processes invlove an Er- and an Yb-ion and energy is transferred from one to the other. If the energy is transferred from the Yb-ion it is called an ET process and if the energy is transferred to the Yb-ion it is called a BET process.
Apart from these processes, we are interested in the interaction, where all energy is transferred from one ion to another ion of the same species, which is in the ground state. This process does not lead to a change in the number of excited states, but it does change the position of the excited states. This eventually leads to an effective diffusion of the excited states. To get a better understanding of how this influences the behaviour of the system, we have reduce this monstrous diagram to a simpler one.
The primary emission of the Er-ions is in the green, which is the sixth energy level in this model. To get here under IR excitation, there is the following main pathway. Photons are being absorbed by the Yb-ions, then one Yb-ion transfers its energy to the Er-ion, with the result that it ends up in state three. After which a second Yb-ion also transfers its energy to the Er-ion, resulting in an ion that is state seven. From here, there is a fast relaxation to the sixth state, where it decays back to the ground state. Since the relaxation from state seven to state six is very fast, we can reduce this Er energy level diagram to a three level diagram, where we only include state one, three and six. To make it as complete as possible, however, we include a CR process, although it does not involve ions in the state three.
We now have a coupled two and three energy level diagrams, there are two ways to reduce this even further, the first option is to split the two species from eachother, such that we either obtain a two level system of solely Yb-ions or a three level system of solely Er-ions. The other option is to merge the coupled system into a single three-level diagram, which can be done, since the excited state of the Yb-ions has the same energy as the third state of the Er-ions. This results in the diagrams as given in figure 2, where a) is the energy diagram of a system solely doped with Yb, b) is the diagram of a system solely doped with Er and c) is a system which is co-doped with both Er and Yb. These last two are the same, but we have to note that the UC process is much faster in the co-doped system.

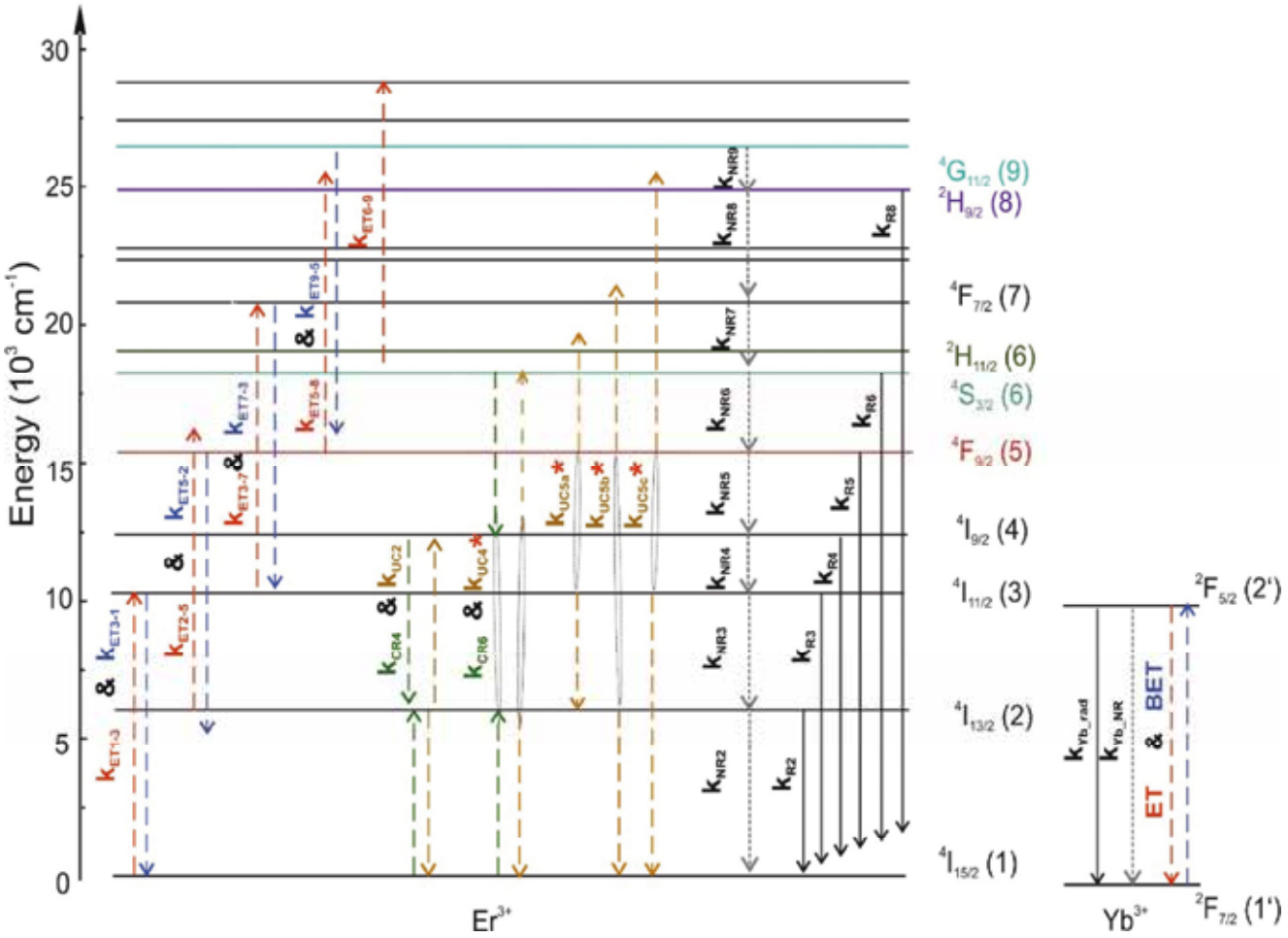

Figure 1: The nine-level energy diagram taken from Kaiser et al.[1] with all different processes. The coloured dotted lines indicate processes which include two ions. The solid lines indicate decay processes with the emission of a photon and the black dotted lines indicate decay processes without the emission of a photon.

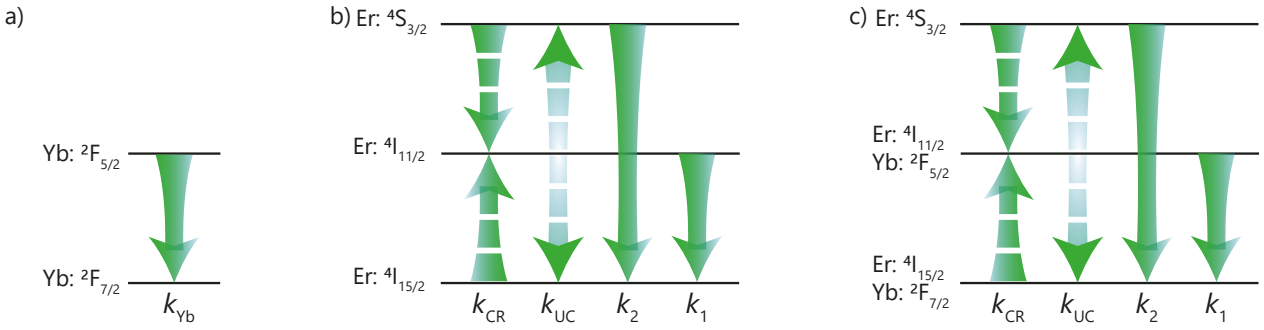

Figure 2: The nine-level energy diagram taken from Kaiser et al.[1] with all different processes. The coloured dotted lines indicate processes which include two ions. The solid lines indicate decay processes with the emission of a photon and the black dotted lines indicate decay processes without the emission of a photon.

2.2 Single dopant energy diffusion

In this section we will study the diffusion of excitations over a single type of dopant in a perfect β-$NaYF_4$ host crystal structure as given in figure 3a. This crystal has the space group $P\bar{6}$ and unit cell parameters $a = b = 5.96606(13)$Å and $c = 3.51738(6)$Å [9]. In this crystal, x% of of the yttrium (Y) sites are randomly substituted for dopants. We assume that these dopants are the only optically active sites, such that excitations can only exist on these doped sites. Furthermore we assume that the excitations can migrate from site to site via a Förster resonance energy transfer process, in which the migration rate can be described as [10]

$$k_{\text{mig}} = \frac{C_{\text{mig}}}{r^6}, \tag{2.1}$$

where C_{mig} is the energy transfer strength and r the distance between the dopants.
To absorb this unknown constant C_{mig} and the size of the unit cell, we use reduces units, which are defined as:

$$r^* = \frac{r}{a}, \tag{2.2}$$

$$t^* = k_{\text{mig},0}t, \text{ where} \tag{2.3}$$

$$k_{\text{mig},0} = \frac{C_{\text{mig}}}{r_0^6}. \tag{2.4}$$

where a is the unit cell length, t is the time, $k_{\text{mig},0}$ is the maximum rate and r_0 is the nearest neighbour distance. In this crystal the nearest neighbour is in the c-direction and can be approximately written by $r_0 = 0.6a$. Using these we can write the non-reduced diffusion coefficient as

$$D = \frac{a^2 C_{\text{mig}}}{r_0^6} D^*, \tag{2.5}$$

where we used that

$$\left\langle (\vec{r} - \vec{r}_0)^2 \right\rangle = 2dDt, \tag{2.6}$$

where $\left\langle (\vec{r} - \vec{r}_0)^2 \right\rangle$ is the mean-squared displacement of an excitation, d the dimensionality in the system. Looking at equation 2.5 we can directly see that the diffusion coefficient depends linearly on the energy-transfer constant C_{mig}.
First we approximate the diffusion coefficient using a mean-field approach. In this approach, we assume that the diffusion coefficient of a single migration is the same as the diffusion coefficient of an infinite amount of migrations. This means we can estimate the mean-squared displacement and migration time as

$$\left\langle (r - r_0)^2 \right\rangle = \frac{\sum_{i \neq j} P(i \to j) \left(\vec{r}_{ij}\right)^2}{N_D} = \sum_{i \neq j} f\left(|\vec{r}_{ij}|\right) \left(\vec{r}_{ij}\right)^2 \text{ and} \tag{2.7}$$

$$\langle t \rangle = \frac{1}{\langle k_{\text{tot}} \rangle} = \frac{N}{\sum_{i \neq j} P_{\text{A}}(j) k_{ij}}, \tag{2.8}$$

where $P(i \to j)$ is the probability to migrate from position i to j, $\vec{r}_{ij}$ is the distance between positions i and j, $f\left(|\vec{r}_{ij}|\right)$ is the frequency that distance $|\vec{r}_{ij}|$ occurs, such that $\sum_{\vec{r}_{ij}} f\left(|\vec{r}_{ij}|\right) = 1$, N_D is the total number of doped sites, k_{ij} is the rate of migration as given in equation 2.1 and $P_A\left(i\right)$ is the probability that position i can accept. We assume that the system is homogeneously distributed, so we can write $P_{\text{A}}\left(i\right) = \phi(1 - \psi)$, with ϕ the ion doping concentration and ψ the excitation doping concentration. Filling this in in equation 2.6 gives us

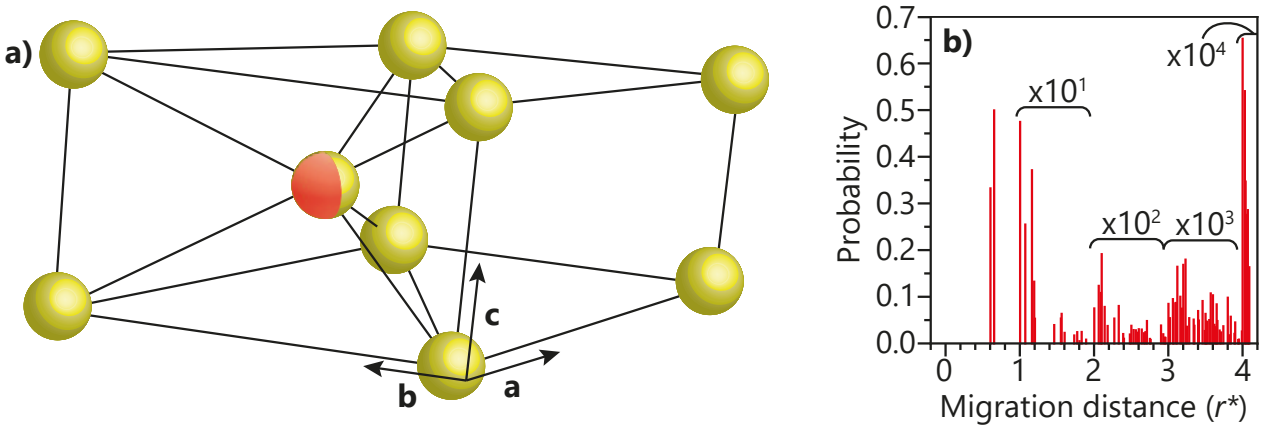

Figure 3: (a) A schematic overview of the yttrium positions in a β-$NaYF_4$ unit cell. The two coloured position is 50% occupied with an yttrium ion. The two positions are at $(0, 0, 0)$ and $(1/3, 2/3, 1/2)$, the angle between $\boldsymbol{a}$ and $\boldsymbol{b}$ is 120° and the unit cell parameters are $a = b = 5.96606(13)$Å and $c = 3.51738(6)$Å [9]. (b) The probability to find an excitation at a distance r^* away after a single migration. Using these probabilities, we can calculate the mean-field diffusion coefficient using equation 2.9.

$$D = \frac{\phi(1-\psi)}{2d} \frac{\sum_{i \neq j} f\left(|\vec{r}_{ij}|\right) \left(\vec{r}_{ij}\right)^2}{\langle t_0 \rangle} \tag{2.9}$$

with $\langle t_0 \rangle$ the average time of a single migration in an ideal 100% doped crystal. From this equation we can directly see that the diffusion coefficient is linearly dependant on both the excitation and ion doping. In figure 3b we show the probability $f(r)$ to migrate a distance r^* away for a single migration step, using equation 2.7 we can approximate the mean-squared displacement for a single migration and using this we can approximate the diffusion coefficient.

2.3 Emission peak broadening for two-level systems

In the next two sections, we connect the effective parameters that follow from the microscopic properties of the crystal to the experiments we will describe later. In these experiments we have a setup that allows us to look at the intensity of the emitted light as a function of time and position and using filters we can separate the emission from the different energy level. Since this emission intensity is linearly dependent on the population in those energy levels, we can measure the number of ions in either of the states independently and more important, the change in this.
To model this, we imagine having an infinitely large 2D sample that contains a homogeneously distributed NCs, which in their turn have a homogeneous distribution of ions with specific energy levels. So effectively we have an infinitely large 2D containing a homogeneous distribution of ions. We also assume that the number of ions at one specific point on that sample is very large, such that we can consider the distribution of ions over the sample to be homogeneous and continuous. This way, we can think of the excited population in terms of a continuum instead of taking into account the discrete number of ions, which allows us to use differential equations to describe the system with.
Now, let us consider a two energy system with a ground state 0 and an excited state 1. In this system the excited population can change in three different ways (see also figure 4a);

1. The ground state population can be excited using an external photon source
2. The excited state can decay back to the ground state.
3. An excited state can transfer its energy to a neighbouring ground state, which effectively results in an diffusion of the excited state.

This we can describe with the following differential equation:

$$\frac{\partial N_1\left(\vec{r},t\right)}{\partial t} = D_1\nabla^2 N_1\left(\vec{r},t\right) + k_{\mathrm{ex},01}(\vec{r},t)N_0\left(\vec{r},t\right) - k_1 N_1\left(\vec{r},t\right), \tag{2.10}$$

where N_i indicates the relative population in state i, such that $\sum_i N_i(\vec{r},t) = 1$, D_i is a diffusion parameter of state i, $k_{\mathrm{ex,ij}}$ is the excitation rate from state i to j and k_i is the decay rate of state i. This equation is not exactly solvable, so we need to make some assumptions. First we will look at the case without diffusion and after that we will look at the case without excitation.
Excitation Saturation If we assume that there is no diffusion, we we can simplify the equation to

$$\frac{\partial N_1\left(\vec{r},t\right)}{\partial t} = k_{\mathrm{ex},01}(\vec{r},t) - \left(k_1 + k_{\mathrm{ex},01}(\vec{r},t)\right)N_1\left(\vec{r},t\right), \tag{2.11}$$

where we used that $N_0(\vec{r},t) = 1 - N_1(\vec{r},t)$. Under the assumption that the excitation parameter does not change over time and is not equal to zero, the solution of this differential equation can be written as

$$N_1(\vec{r},t) = \frac{1}{1 + k_1/k_{\mathrm{ex},01}(\vec{r})}\left(1 - \mathrm{e}^{-(k_{\mathrm{ex},01}(\vec{r})+k_1)t}\right). \tag{2.12}$$

In this equation we see that the population changes exponentially over time with the two important limits being $t \to 0$ and $t \to \infty$. In this first limit, the behaviour is predominantly determined by the excitation, and in the second limit, the system has reached a steady-state solution where the excitation and decay are in equilibrium with each-other. These can be written as

$$\lim_{t\to 0} N_1(\vec{r},t) = \frac{k_{\mathrm{ex},01}(\vec{r})}{k_{\mathrm{ex},01}(\vec{r}) + k_1}\left(1 - 1 + (k_{\mathrm{ex},01}(\vec{r}) + k_1)t\right) = k_{\mathrm{ex},01}(\vec{r})t \tag{2.13}$$

$$\lim_{t\to\infty} N_1(\vec{r},t) = \frac{1}{1 + k_1/k_{\mathrm{ex},01}(\vec{r})}. \tag{2.14}$$

In order to study this equation in terms of excitation power, we will derive a relationship between the excitation parameter $k_{\mathrm{ex},01}$ and the excitation power P. For this we use the knowledge that every excitation occurs upon absorbing a photon, so $\mathrm{d}N_1 = \mathrm{d}N_{\mathrm{ph}}$, where N_{ph} is the number of photons,. For the change of excited stated due to excitation $\mathrm{d}N_1$, we use the excitation part of equation 2.10. For the change of photons we use that for a single photon the probability to 'hit' an ion and be absorbed per distance $\mathrm{d}z$ traveled through the medium is equal to the volume density ρ_0 of the ground-state ions N_0 times the absorption cross-section σ_{01}. In equation-form this reads

$$\mathrm{d}N_1(\vec{r},t) = k_{\mathrm{ex},01}(\vec{r},t)N_0(\vec{r},t)\mathrm{d}t, \tag{2.15}$$
$$\mathrm{d}N_{\mathrm{ph}}(\vec{r},t) = -N_{\mathrm{ph}}(\vec{r},t)\rho_0\sigma_{01}\mathrm{d}z, \tag{2.16}$$

Using that $N_{\mathrm{ph}}(\vec{r},t)E_{\mathrm{ph}}/\left(At\right) = I(\vec{r},t)$, where $E_{\mathrm{ph}} = \frac{hc}{\lambda}$ is the energy per photon, h is Planck's constant, c is the speed of light, λ is the photon wavelength, A is the area and $I(\vec{r},t)$ is the excitation intensity, gives

$$k_{\mathrm{ex},01}(\vec{r},t) = \frac{I(\vec{r},t)\sigma_{01}\lambda}{hc}, \tag{2.17}$$

We can also write $I(\vec{r},t) = I_{\max}(t)f(\vec{r})$, where $I_{\max}(t)$ is the amplitude of the excitation intensity and $f(\vec{r})$ is the shape. From this we can calculate the excitation power $P(t) = \int_A I_{\max}(t)f(\vec{r})\mathrm{d}A$. Filling this all in gives

$$k_{\mathrm{ex},01}(\vec{r},t) = \frac{P(t)\sigma_{01}\lambda}{hc\int_A f(\vec{r})\mathrm{d}A}f(\vec{r}) \tag{2.18}$$
$$k_{\mathrm{ex},01}(\vec{r},t) = C_{\mathrm{ex},01}P(t)f(\vec{r}). \tag{2.19}$$

where we define

$$C_{\mathrm{ex},01} = \frac{\sigma_{01}\lambda}{hc\int_A f(\vec{r})\mathrm{d}A} \tag{2.20}$$

Filling this in in equations 2.13 and 2.14 and using that the emission intensity depends linearly on the number of excited states $I_{\mathrm{em}} = C_{\mathrm{em}}N_1$, we find that

$$\lim_{t\to 0} I_{\mathrm{em}} = C_{\mathrm{em}}C_{\mathrm{ex},01}Pf(\vec{r})t \tag{2.21}$$
$$\lim_{t\to \infty} I_{\mathrm{em}} = \frac{C_{\mathrm{em}}}{1+\frac{k_1}{C_{\mathrm{ex},01}Pf(\vec{r})}}. \tag{2.22}$$

Here we note that at very short times, the shape of the emission intensity profile is the same as that of the excitation intensity profile, independent of the power. At very long times, however, we see that the shape of the emission peak depends on the power. At very low powers, we can neglect the 1+ in the denominator, giving again the same shape, while at very high powers, the emission intensity profile becomes a constant value over the whole area. This thus means that the steady-state emission profile broadens without diffusion due to saturation effects.
In order to see more clearly how this the emission intensity, we will work this equation out for two different excitation intensity profiles. First we will look at a laser profile that is Lorentzian, because this is the profile that we observed in our experiments. And second, we will look at a laser excitation profile that is Gaussian shaped in order to show the difference with a profile that is more steeply shaped. So first, let us assume that the laser profile has a Lorentzian shape of the form $f(\vec{r}) = \left(1+\left(\frac{\vec{r}}{\gamma}\right)^2\right)^{-1}$. Filling this in equation 2.22 gives

$$\lim_{t\to\infty} I_{\text{em}} = \frac{C_{\text{em}}}{1+\frac{k_1}{C_{\text{ex},01}P}\left(1+\left(\frac{\vec{r}}{\gamma}\right)^2\right)} \tag{2.23}$$

$$= \frac{C_{\text{em}}C_{\text{ex},01}P}{C_{\text{ex},01}P+k_1}\frac{1}{1+\frac{r^2}{\gamma'^2}}, \text{with} \tag{2.24}$$

$$\gamma'^2 = \left(1+\frac{C_{\text{ex},01}P}{k_1}\right)\gamma^2. \tag{2.25}$$

Where we define γ' as the width of the emission intensity profile and γ as the width of the excitation intensity profile. The relative width in this case, we define as γ'/γ. From this we see that in a steady state a Lorentzian excitation profile induces a Lorentzian emission profile with a different width, where this width depends on the power. This means that we can find the cross-section by measuring the emission widths of a steady state as a function of power.

When we assume a Gaussian excitation profile $f(\vec{r}) = e^{-\frac{r^2}{2s^2}}$, the steady-state emission profile cannot be written as a Gaussian function, so here we need a different method of comparing the steady-state emission profile and the excitation profile. For this we define the width for these, we use the square root of the variance s', which reduces to s for the excitation profile. Furthermore, we define the relative width as s'/s, so this becomes

$$s'^2 = \text{Var}\left(\lim_{t\to\infty} I_{\text{em}}\right) \tag{2.26}$$

$$= \text{Var}\left(\frac{C_{\text{ex},01}}{1+\frac{k_1}{C_{\text{ex},01}P}\exp\left(\frac{r^2}{2s^2}\right)}\right) \tag{2.27}$$

$$= -\frac{\text{Li}_2\left(-\frac{C_{\text{ex},01}P}{k_1}\right)}{\ln\left(1+\frac{C_{\text{ex},01}P}{k_1}\right)}2s^2, \tag{2.28}$$

where $\text{Li}_n(x)$ is the polylogarithmic function.

In order to see how these emission intensities broaden and to compare the broadening of the Lorentzian and Gaussian excitation profiles, we show in figure 4b the relative width as a function of the relative power. In this figure, we see that a Lorentzian shaped power distribution broadens much faster than a Gaussian shaped one. Furthermore, we show the shapes of the broadened Lorentzian and Gaussian shapes at a relative power of 100, where we see that the Lorentzian broadens primarily its tails, while a Gaussian broadens its peak.

Diffusion Apart from this broadening effect that occurs due to saturation, we can also look at the broadening effect that occurs due to diffusion. So let us consider the case that there is diffusion. In this case, we simplify the equation by setting the excitation parameter to zero, which is the situation after the laser is turned off. This reduces equation 2.10 to

$$\frac{\partial N_1(\vec{r},t)}{\partial t} = D\nabla^2 N_1(\vec{r},t) - k_1 N_1(\vec{r},t). \tag{2.29}$$

From this equation we see that the only term that changes the shape and width of the emission profile is the diffusive term and the only term that changes the overall amplitude is the decay term. This thus means that the emission profile is the convolution between the initial profile and a Gaussian distribution with a variance of $s^2 = 2dDt$, where d is the number of dimensions and t is the time with respect to the initial profile. The overall amplitude is a exponential decay of the initial amplitude $\frac{A_1(t)}{A_1(0)} = e^{-k_1 t}$, with $A_1(t)$ the amplitude at time t. We can thus write the total solution as

$$N_1(\vec{r},t) = \frac{e^{-k_1 t}}{(4\pi dDt)^{\frac{d}{2}}}\int_{-\infty}^{\infty} N_1\left(\vec{R},0\right)e^{-\frac{(\vec{r}-\vec{R})^2}{4dDt}}\mathrm{d}\vec{R}. \tag{2.30}$$

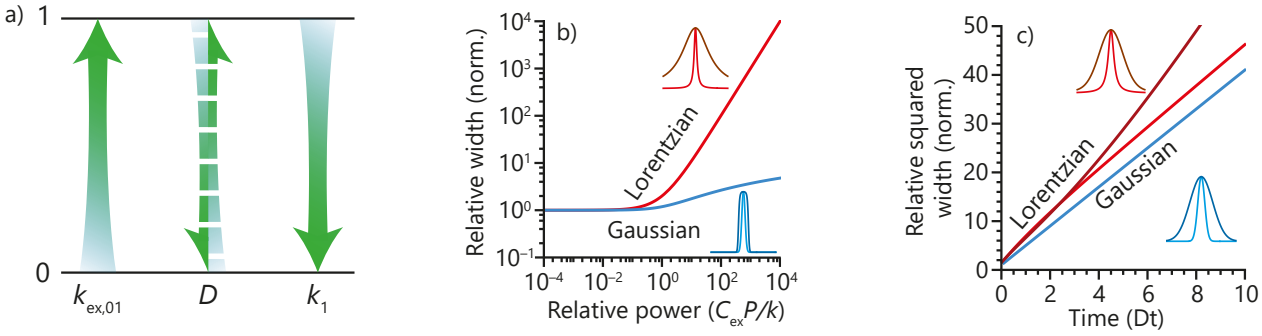

Figure 4: a) The different processes involved in the two level system; the excitation from the ground state to the excited state with a rate $k_{\mathrm{ex},01}$, the energy transfer where the excited state effectively diffuses with a diffusion coefficient D and the decay of the excited state to the ground state with a rate k_1. b) The relative widths of a Lorentzian- (red) and Gaussian-excited (blue) emission intensity profile as an function of the relative power $\frac{C_{\mathrm{ex},01}P}{k_1}$. Here the relative width is defined as γ'/γ and s'/s from equations 2.25 and 2.28 respectively. We see that a Lorentzian profile broadens much faster than the Gaussian shaped profile. This is also illustrated in the small profiles above and below the lines, where the upper profile is a Lorentzian and the lower profile is a Gaussian, the bright lines indicate the excitation profiles and the dark lines indicate the emission profiles at a relative power of 100. Here we see that a Lorentzian emission profile broadens over the whole regime, but the Gaussian shaped profile broadens mostly at the top. c) The relative squared width of an initial Gaussian (blue) or Lorentzian (red) profile as a function of the diffusion time Dt, which is normalized, such that the width at $Dt = 0$ equals one. This width is defined using a Gaussian fit. In addition to defining the width using a Gaussian fit, we can also estimate the width of the Lorentzian initial profile using a Lorentzian fit (dark-red). We also show to intensity profiles at $Dt = 0$ (light) and $Dt = 5$ (dark) as insets in red (Lorentzian) and blue (Gaussian). From these insets we see that the profile becomes Gaussian in both cases. This means that at larger diffusion times, it would probably be more accurate to quantify the width using a Gaussian fit. This can also be seen in the width, where the Lorentzian fit to a Lorentzian-diffusion has a much larger slope and thus overestimates the diffusion coefficient.

In the case that $N_1(\vec{r}, 0)$ is a Gaussian profile with an initial width σ_0, we know that the solution of the diffusion equation is a Gaussian with a width of $\sigma^2 = 2dDt + \sigma_0^2$, where d is the number dimensions and D is the diffusion coefficient. In the case that the initial position is a Lorentzian profile with an initial width γ_0, however, we find that the solution is a Voigt distribution [11], which equals the real part of a complex function. Since it is not trivial to fit a complex function, we approximate the width with both a Gaussian and a Lorentzian fit and we define the width as either the standard deviation or the γ-parameter, respectively, since the initial profile looks more like a Lorentzian and the profile at large times looks more like a Gaussian as can also be seen in the upper inset in figure 4c.
In this figure we also show the relative squared width of a diffusing Gaussian in blue and the width of a diffusing Lorentzian calculated using a width defined using either a Gaussian or a Lorentzian fit in respectively light-red and dark-red. We see that at small diffusion times, the slopes of all curves are approximately the same, but at larger diffusion times, the width of the Lorentzian initial profile calculated using a Lorentzian fit increases much faster than the other two curves. The reason for this is that the initial Lorentzian profile broadens to a Gaussian shape and a Lorentzian fit fails in capturing the width of that shape.

2.4 Emission peak broadening for three-level systems

We now consider a three-level system, which we again assume to be continuous, such that we can use differential equations. In this system, we have 3 states, 0, 1 and 2, where the energy difference between state 0 and 1 is equal to the energy difference between state 1 and 2. The population in these states can change due to the following processes;

1. An ion in state i can be excited to another state j with a higher energy by a photon with an energy that corresponds to the energy difference between those two states, with a rate of $k_{\text{ex,ij}}$. We can thus tune these parameters by tuning the flux of photons. If our excitation source (laser) gives photons of the energy that corresponds to the energy difference of state 0 and 2, the rates $k_{\text{ex,01}}$ and $k_{\text{ex,12}}$ equal 0 and if the laser gives photons of energy that corresponds to the energy difference between state 0 and 1, thus also 1 and 2, the rate $k_{\text{ex,02}} = 0$.
2. There is also a probability that an ion in the excited state interacts with an ion in the ground state and all energy is transferred from the excited ion to the ground-state ion. This results in an effective diffusion of that state, with a diffusion coefficient D_{i}.
3. Another possibility is that the only part of the energy transfers, which is called a cross-relaxation process. Here an ion in state 2 interacts with an ion in state 0 and as a result there are two ions in state 1, this happens with a rate k_{CR}.
4. It is also possible to have the reverse process, where two ions in state 1 combine to one ion in state 2 and one ion in state 0. This is called an upconversion process and happens with a rate k_{UC}.
5. Lastly there is the probability for an ion to decay back to the ground state, where a state i decays to the ground state under emission of a photon, which happens with a rate k_{i}.

This we write as the following system of differential equations

$$\frac{\partial N_2\left(\vec{r},t\right)}{\partial t} = D_2\nabla^2 N_2\left(\vec{r},t\right) + k_{\text{ex,02}}(\vec{r},t)N_0\left(\vec{r},t\right) + k_{\text{ex,12}}(\vec{r},t)N_1\left(\vec{r},t\right) - k_{\text{CR}}N_0N_2 + k_{\text{UC}}N_1^2 - k_2N_2, \tag{2.31}$$

$$\frac{\partial N_1\left(\vec{r},t\right)}{\partial t} = D_1\nabla^2 N_1\left(\vec{r},t\right) + k_{\text{ex,01}}(\vec{r},t)N_0\left(\vec{r},t\right) - k_{\text{ex,12}}(\vec{r},t)N_1\left(\vec{r},t\right) + 2k_{\text{CR}}N_0N_2 - 2k_{\text{UC}}N_1^2 - k_1N_1, \tag{2.32}$$

We consider the case that there is no diffusion and there is no excitation source, since this allows us to simplify and solve the equations analytically. This reduces the equations to

$$\frac{\partial N_2\left(\vec{r},t\right)}{\partial t} = -k_{\text{CR}}N_0N_2 + k_{\text{UC}}N_1^2 - k_2N_2, \tag{2.33}$$

$$\frac{\partial N_1\left(\vec{r},t\right)}{\partial t} = 2k_{\text{CR}}N_0N_2 - 2k_{\text{UC}}N_1^2 - k_1N_1. \tag{2.34}$$

In these equations we can differentiate two limits, the upconversion term is much larger than the cross relaxation term or the other way around. One way to find this behaviour, is to have an initial population solely in the N_2 and N_1 respectively. In other words we have the case that $k_{\text{CR}}N_0N_2 >> k_{\text{UC}}N_1^2$ when $N_1 \approx 0$ and that $k_{\text{CR}}N_0N_2 << k_{\text{UC}}N_1^2$ when $N_2 \approx 0$.
First we look at the case where the cross-relaxation is the dominant term, $k_{\text{CR}}N_0N_2 >> k_{\text{UC}}N_1^2$ and $N_1 \approx 0$, which yields,

$$\frac{\partial N_2\left(\vec{r},t\right)}{\partial t} = -k_{\text{CR}}(1-N_2)N_2 - k_2N_2, \tag{2.35}$$

$$\frac{\partial N_1\left(\vec{r},t\right)}{\partial t} = 2k_{\text{CR}}(1-N_2)N_2 - k_1N_1. \tag{2.36}$$

In this equations we see that the differential equation of state 2 is no longer coupled to the differential equation of state 1 and its solution can be written as

$$N_2\left(\vec{r},t\right) = c_2^{-1}e^{-kt}\left(c_2^{-1}N_2^{-1}\left(\vec{r},0\right) - 1 + e^{-kt}\right)^{-1}, \tag{2.37}$$

where $c_2 = \frac{k_{\mathrm{CR}}}{k}$ and $k = k_2 + k_{\mathrm{CR}}$. We see that the positional dependence is solely in the denominator, which gives rise to the idea that an initial Lorentzian-shaped N_2-profile will stay a Lorentzian shaped profile, but with a different width. So as the initial profile we use

$$N_2\left(\vec{r},0\right) = A_2\left(1 + \left(\frac{\vec{r}}{\gamma_2}\right)^2\right)^{-1}, \tag{2.38}$$

where A_2 is the amplitude of the profile between 0 and 1 and γ_2 is the width of the profile. Filling this in in equation 2.37, yields

$$N_2\left(\vec{r},t\right) = \frac{A_2e^{-kt}}{1 - A_2c_2(1-e^{-kt})}\left(1 + \frac{1}{1 - c_2A_2(1-e^{-kt})}\left(\frac{\vec{r}}{\gamma_2}\right)^2\right)^{-1} \tag{2.39}$$

$$= A_2'\left(t\right)\left(1 + \left(\frac{\vec{r}}{\gamma_2'}\right)^2\right)^{-1}, \tag{2.40}$$

with,

$$\gamma_2'^2 = (1 - A_2c_2(1-e^{-kt}))\gamma_2^2 \tag{2.41}$$

$$A_2'\left(t\right) = \frac{e^{-kt}}{1 - A_2c_2(1-e^{-kt})}A_2. \tag{2.42}$$

From this equations, we thus see that an initial Lorentzian profile leads to a narrower Lorentzian profile as a result of a cross-relaxation process. This can be understood by considering the cross-relaxing decay process relative to the N_2 population, $\frac{k_{\mathrm{CR}}N_0N_2}{N_2} = k_{\mathrm{CR}}N_0$. Here we see that the relative decay only depends on the N_0 population, which can be written as $N_0 = 1 - N_2$ and where N_2 has a peak, N_0 has thus a valley. This means that the relative decay is faster at the tails of the population distribution than it is at the peak. We also see that this effect becomes larger when the peak of N_2 becomes larger, as we also found in equation 2.41.
In order to see how what this behaviour looks like, we show the width of the population in the state N_2 as a function of the relative time kt at increasing values of A_2c_2. We see that upon increasing this value, the effect of narrowing becomes larger, as we expected. We also see that the time-scale upon which this effect happens is the same as the one upon which the population decays.
In the other case, where the up-conversion is the dominant term, $k_{\mathrm{CR}}N_0N_2 << k_{\mathrm{UC}}N_1^2$ and $N_2 \approx 0$, we can simplify equations 2.33 and 2.34 to

$$\frac{\partial N_2\left(\vec{r},t\right)}{\partial t} = k_{\mathrm{UC}}N_1^2 - k_2N_2, \tag{2.43}$$

$$\frac{\partial N_1\left(\vec{r},t\right)}{\partial t} = -2k_{\mathrm{UC}}N_1^2 - k_1N_1. \tag{2.44}$$

Here we, again, see that the differential equation of state 1 does no longer depend on the population is state 2 and solving this equation yields

$$N_1\left(\vec{r},t\right) = e^{-k_1t}\left(c_1^{-1}N_2^{-1}\left(\vec{r},0\right) + 1 - e^{-k_1t}\right)^{-1}, \tag{2.45}$$

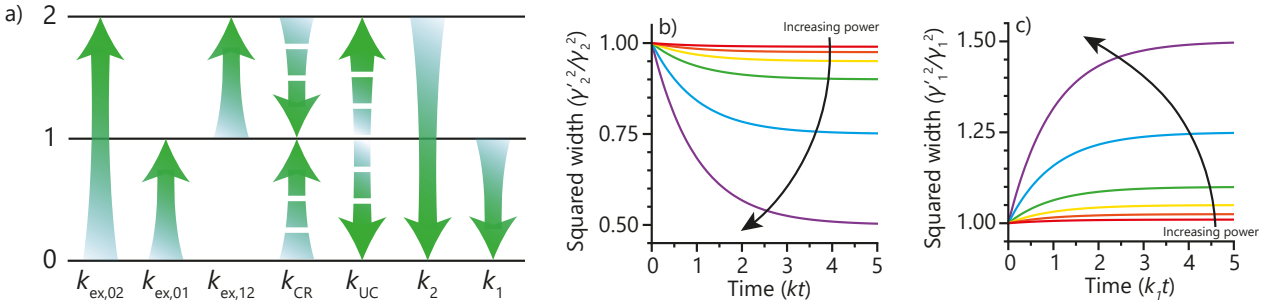

Figure 5: a) The different processes we consider in our three-level system, with equal energy spacing; first of all we have the different different exciting processes with rates $k_{\text{ex,ij}}$, where ij indicates states of the transition. Next we have the processes that includes the interaction between two states, the cross-relaxation process with a rate of k_{CR} and the up-conversion process with a rate of k_{UC}. In these processes a 0-state and a 2-state combine two 1-states or vise-versa, respectively. Lastly we also have the decay processes, where the exited state decays back to the ground state, with a rate k_{i}. In this figure we do not display the diffusion processes, which is an effect of a combination of states i and j to states j and i, resulting in an effective energy diffusion. b) and c) Respectively, the squared width relative to the initial N_2-profile width as a function of the relative time kt due to cross-relaxation and the squared width relative to the initial N_1-profile width as a function of the relative time k_1t due to up-conversion. The lines indicate, respectively A_2c_2 and $A_1c_1 = 0.001$ (red), 0.025 (orange), 0.05 (yellow), 0.01 (green), 0.025 (blue), 0.05 (purple). At the same sample, this increase in this value can be seen as a increase in power, as also indicated in the figures. We see that the upon increasing the power (A_ic_i-value), the effect of broadening or narrowing is increased. Furthermore, we see that the time-scale on which this happens is the same time-scale upon which the decay processes happen.

where $c_1 = \frac{2k_{\text{UC}}}{k_1}$. We see that this equation looks very similar to equation 2.37. So we take the same initial profile, such that

$$N_1\left(\vec{r},0\right) = A_1\left(1+\left(\frac{\vec{r}}{\gamma_1}\right)^2\right)^{-1}, \tag{2.46}$$

where A_1 is the amplitude of the profile between 0 and 1 and γ_1 is the width of the profile. Filling this in in equation 2.45, yields

$$N_1\left(\vec{r},t\right) = \frac{A_1e^{-k_1t}}{1+c_1A_1(1-e^{-k_1t})}\left(1+\frac{1}{1+c_1A_1(1-e^{-k_1t})}\left(\frac{\vec{r}}{\gamma_1}\right)^2\right)^{-1} \tag{2.47}$$

$$= A_1'\left(t\right)\left(1+\left(\frac{\vec{r}}{\gamma_1'}\right)^2\right)^{-1}, \text{ with} \tag{2.48}$$

$$\gamma_1'^2\left(t\right) = \left(1+c_1A_1\left(1-e^{-k_1t}\right)\right)\gamma_1^2 \text{ and} \tag{2.49}$$

$$A_1'\left(t\right) = \frac{e^{-k_1t}}{1+c_1A_1\left(1-e^{-k_1t}\right)}A_1 \tag{2.50}$$

From this equations we see the opposite effect as we saw in the cross-relaxation case, in this case, we see that the Lorentzian profile broadens and this effect increases upon increasing the value of A_1c_1, as we also show in figure 5c. These effects can be explained by looking at the up-conversion decay of the N_1 population relative to its population, $\frac{2k_{\text{UC}}N_1^2}{N_1} = 2k_{\text{UC}}N_1$. In this equation, we see that there is a faster decay at the N_1 peak than at tails, which means that the distribution will broaden. We also see that this effect is larger when the N_1 population is larger, so upon increasing the amplitude of the initial population, the broadening effect also increases.

In both equations we see that the broadening behaviour depends on the the amplitude of the initial profile, so it is useful to have some approximate expression for this amplitude. This we do with the approximation that we excite very short, such that this timescale is much shorter than the ones in which cross-relaxation and up-conversion happen. This means that we can neglect these processes and reduce the system as a two-level system with only an excitation and decay process. Which gives the following differential equations:

$$\frac{\partial N_{\mathrm{i}}}{\partial t} = k_{\mathrm{ex,0i}} N_0 - k_{\mathrm{i}} N_{\mathrm{i}}. \tag{2.51}$$

Using that $N_0 = 1 - N_{\mathrm{i}}$, the solution of this equation becomes:

$$N_{\mathrm{i}} = \frac{k_{\mathrm{ex,0i}}}{k} \left(1 - e^{-k t_{\mathrm{ex}}}\right) \tag{2.52}$$

where $k = k_{\mathrm{ex,0i}} + k_{\mathrm{i}}$ and t_{ex} is the duration of the excitation pulse. In the limit that $kt_{\mathrm{ex}} << 1$, we can further approximate this to

$$\lim_{k t_{\mathrm{ex}} \to 0} N_{\mathrm{i}} = \frac{k_{\mathrm{ex,0i}}}{k} \left(1 - 1 + k t_{\mathrm{ex}}\right) = k_{\mathrm{ex,0i}} t_{\mathrm{ex}} \tag{2.53}$$

Filling in the relation between the excitation parameter and the fundamental constants, as we found in 2.18, we find

$$\lim_{k t_{\mathrm{ex}} \to 0} N_{\mathrm{i}} = \frac{\sigma_{0i} \lambda}{hc \int_A f(\vec{r}) \mathrm{d}A} f(\vec{r}) P t_{\mathrm{ex}} \tag{2.54}$$

From this equation we see that we can tune the amplitude of the initial profile, which will increase the broadening and narrowing effect of the emission peaks. Upon increasing the product Pt_{ex}, we increase the broadening and narrowing effect as also shown in figures 5b an 5c.

3 Methods

3.1 Monte Carlo simulation of diffusion on a lattice

In this section, we will discuss the Monte Carlo simulation that we use to find an effective diffusion coefficient for energy migrating over a lattice. The simulation consists of two different parts, first we have the initialization phase where we initialize the structure and secondly we have the simulation phase where we let the excitations migrate.
The initialization has the following steps:

1. Determine all possible positions where an excitation can be found. In our system these are the yttrium positions that have been replaced with an ytterbium. To do this we use a two step system, where we first determine all yttrium positions and then replace each of them by an ytterbium with a probability of ϕ, where ϕ is the ytterbium doping fraction.

2. Next we calculate the migration rates for all possible energy transfers. This we do by looping over all lattice sites, where we determine all neighbours within a cut-off radius of $4.1r^*$. For all these neighbours we calculate the rate k using 2.1 and normalize them such that the maximum possible rate k_0 equals 1. In our case this is a migration to the nearest neighbour in the $\boldsymbol{c}$-direction. The normalized rate then becomes

$$k^* = k/k_0 = \left(\frac{r_0}{r}\right)^6 \tag{3.1}$$

3. The last step in the initialization consists of placing the excitations on the structure. We do this randomly by looping over all possible position and excite them with a probability of ψ, where ψ is the energy doping fraction.

For the simulation itself we define a step as N moves, where N is the number of excitations, of:

1. Pick a random excitation and target, which is one of the neighbours of the hosting ytterbium.

2. Check whether there is already an excitation present, if so reject the move.

3. Accept or reject this move with a probability equal to the normalized rate.

4. Add a time of $\Delta t = 1/M$, where M is the number of possible moves, which is the number of neighbours in this case.

3.2 Synthesis of $NaYF_4$ nanocrystals

In this section we will describe the synthesis of $NaY_{1-x-y}F_4$:$Er^{3+}_x Yb^{3+}_y$-nanoparticles, where x and y indicate the fraction of Er and Yb respectively. In this synthesis the nanocrystals (NCs) are prepared via a co-precipitation method as described by R. Geitenbeek et al. [4].

Chemicals

The following chemicals were used without further purification:

- 1 mmol of lanthanide acetate hydrates (99.9%, $Ln(Ac)_3$) with an Y:Er:Yb ratio of $1-x-y:x:y$, so for a doping of 2%Er 18%Yb the ratio becomes $80:2:18$.
- 6 mL oleic Acid (90%, OA)
- 17 mL 1-octadecene (90%, ODE)
- 2.5 mmol sodium hydroxide (> 97%, NaOH)
- 4 mmol ammonium fluoride (> 98%, NH_4F)
- 10 mL methanol (> 99.85%, MeOH)
- 50 mL ethanol (> 99.8%, EtOH)
- 30 mL cyclohexane (99.5%, CH)

Synthesis

The synthesis can be divided into two phases, the nucleation phase and the growth phase. During the nucleation the reaction mixture is kept at room temperature to prevent the formation of hazardous byproducts such as HF. These byproducts form at elevated temperatures, because of the decomposition of the NH_4F. Once all of this precursor is used to form sub-10nm cubic $NaYF_4$ nuclei, the growth phase is initiated by increasing the temperature. During this growth phase, the small nuclei form larger hexagonal crystals via Ostwald ripening-like growth.

The synthesis is performed in a Schlenk-line setup to work under N_2 and vacuum. And during the reaction, the reactants are stirred vigorously.

The nucleation phase

- First, the $Ln(Ac)_3$ are added to a mixture of the OA and the ODE.
- This white, turbid dispersion is degassed under vacuum at 120 °C for 90 min, resulting in a clear, yellowish solution.
- The mixture is flushed three times with vacuum and N_2 to remove any remanent oxygen and water. After the flushing the mixture, now under N_2 is cooled down to room temperature.
- The Na and F precursors are prepared by dissolving the NaOH and NH_4F in 2.5 mL and 7.5 mL MeOH, respectively.
- When the reaction mixture is at room temperature, the precursors are quickly added to the reactant to supress any oxygen and water flowing in. The result is again a white, turbid mixture.
- The mixture is stirred for approximately 16 h to form the small cubic NCs.

The growth phase

- Before the growth is initiated, the excess MeOH is removed. This is done by slowly heating the mixture under vacuum to 100 °C for 30 min. The best way to do this is to heat the mixture first to 50 °C before putting the mixture under vacuum.
- Next the mixture is flushed three times with N_2 and vacuum.

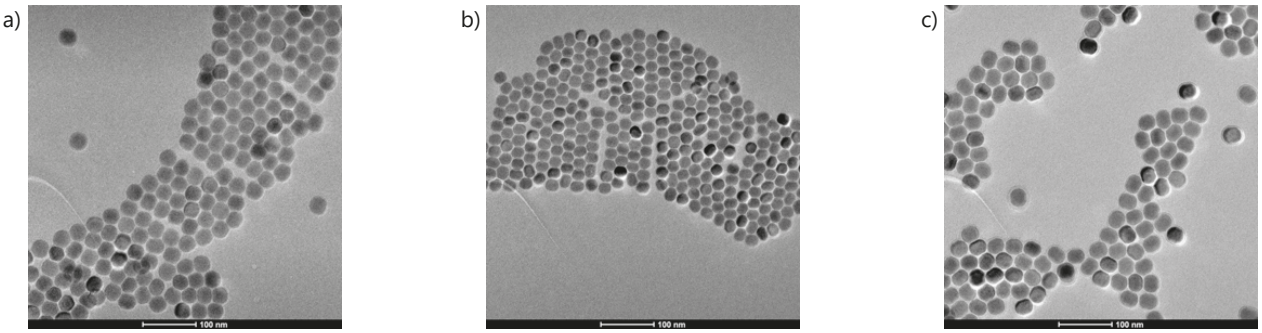

Figure 6: TEM images of the different synthesized nanocrystals, which are doped with (a) 18%Yb, (b) 2%Er and (c) 18%Yb 2%Er.

- The mixture is heated under N_2 to 300 °C for 110 min, which result in the larger hexagonal NCs. After this a light-brown clear solution is obtained, where the brown colour is a result of the oxidation of a small fraction of the organic molecules.
- The mixture is cooled down to room temperature and becomes slightly turbid.

The wash phase

- 1 equivalent EtOH is added to the mixture, which is then centrifuged with 840 relative centrifugal force (RCF) for 8 min.
- The supernatant is removed, after which it is redispersed in 10 mL CH.
- These washing steps are repeated two more times to obtain a clear, colorless dispersion of the NCs.

In figure 6 we show the TEM images of the synthesized nanocrystals. Which have doping concentrations of (a) 18%Yb, (b) 2%Er and (c) 18%Yb 2%Er in order to be able to separate the different energy levels and simplify the energy level system. We see that all nanocrystals have approximately the same size and shape. In order to make the samples for the experimental setup, we made thin films of this by spincoating a drop of these solutions on a cover slip and taping it on a microscope slide.

3.3 Spatial dependant setup

In this section, we will discuss the setup we use to study the temporal and spatial behaviour of the emission intensity. This is done using the setup given in figure 7a. First, we have laser, which emits light with the wavelength needed to excite the sample to the preferred energy level. The light will then arrive of the beam expander, which consists of two lenses with a different focus distance. The first lens focuses the collimated light and the second lens then again collimates the light. The length of this beam expander is the focusing distance of the first lens f_1 plus the focusing distance of the second lens f_2 and the width of the laser beam has expanded with a factor $\frac{f_2}{f_1}$. This beam expander is used in order to minimize the profile width on the sample, which is otherwise broadened due to the diffraction limit. After the beam expander, the light beam hits a dichroic mirror, which is chosen such that the laser light is reflected towards the microscope objective. This objective then focuses the light beam on the sample, which is then excited and emits light of its own. That light is then collimated by the objective and this wavelength passes through the dichroic mirror to be reflected by the galvo mirror, which oscillates due to a voltage, and be focused by the final lens. This focused light is detected by the single photon detector, which sends a signal every time it registers a photon. This signal is detected by the sync box and converters it to a timestamp. This sync box also collects the timestamps for the beginning of a laser pulse and the start of an oscillation of the galvo mirror. The output of this sync box are three lists of these timestamps. From these timestamps we can calculate the time of a photon with respect to the start of a laser pulse and with respect to the start of an oscillation of the galvo mirror.
In figure 7 we show a schematic overview of how we can scan the spatial distribution of the emission intensity. The light that is emitted from the sample, hits the lens, which collimates it. This collimated beam, however, has a different angle θ at different positions. This can be seen by using the properties of a perfect lens, it focuses a colimated beam to a point on the focal plane and a point source of light at the focal plane is colimated. When we only look at the central rays, we can see those as colimated, thus they are focused to the focal point. We know that the rays from the same point are colimated, so the beam is still colimated, but it has a slightly different angle $\theta_{\text{out}} = -\arctan\frac{x}{f}$, which is the angle with respect to the normal and x is the position on the sample and f is the focal length of the lens.
The light beams are then redirected by the galvo mirror and because of this different incoming angle, we can tune which of the two beams will hit the centre of the lens and as a result is detected by the APD. One can show using basic geometry and under the assumption that the beams have sufficiently small angles, such that they are centered on the centre of the galvo mirror, that $x = -f\tan 2\theta_{\text{m}}$, where θ_m is the angle of the galvo mirror, chosen such that it is symmetric in θ_{m}. At sufficiently small angles, this reduces to $x = -2f\theta_{\text{m}}$. Furthermore, the angle of the galvo mirror scales linearly with the applied voltage V_{m}, so we can write that $x = \alpha V_{\text{m}}$, where α is the conversion factor. In order to scan the entire plane of the sample, we let the voltage oscillate with an triangular wave, such that

$$x = \begin{cases} \frac{t_{\text{m}}}{\frac{1}{4}p}\alpha V_{\max} & 0 \le t_{\text{m}} < \frac{1}{4}p \\ -\frac{t_{\text{m}}-\frac{1}{2}p}{\frac{1}{4}p}\alpha V_{\max} & \frac{1}{4}p \le t_{\text{m}} < \frac{3}{4}p \\ \frac{t_{\text{m}}-p}{\frac{1}{4}p}\alpha V_{\max} & \frac{3}{4}p \le t_{\text{m}} < p \end{cases} \tag{3.2}$$

where t_{m} is the time with respect to the start of the oscillation, p is the period of the oscillation and $V_{\max}$ is the voltage amplitude. In order to find the conversion factor α, we perform a calibration, where we send the emission to a camera of which we exactly know the pixel size and to the APD. For both methods we determine the centre of the emission and repeat the process for the different positions of the excitation on the sample. These results are shown in figure 7c. Fitting a line through this data gives the conversion factor $\alpha = 0.30$ µm mV^{-1}.

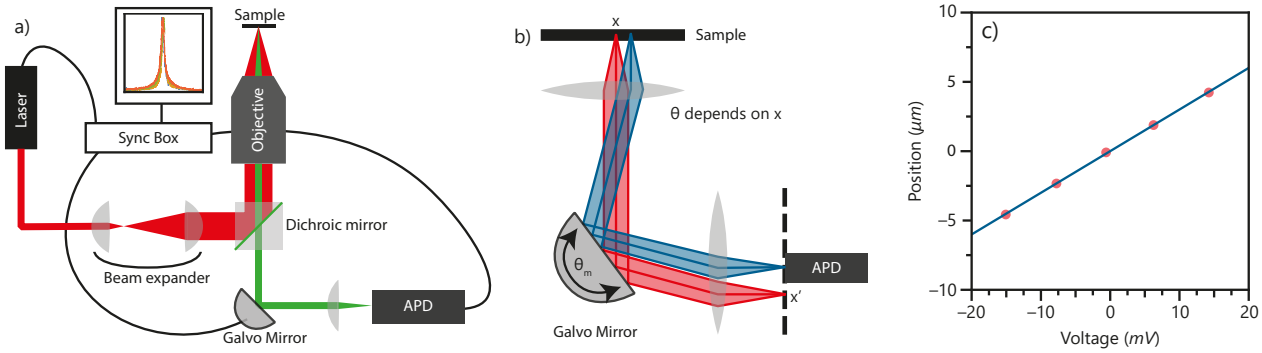

Figure 7: a) A schematic overview of the setup. A laser beam is focused on the sample using a microscope objective, after which the sample emits light at a different wavelength. The reflection of the laser beam and the emitted light go back through objective and are separated using a dichroic mirror or a combination of filters. The emission light passes through on the galvo mirror, which can be rotated using an input voltage. After this a single photon detector (APD) detects single photons and sends a signal digital signal to the sync box, where the timing is synchronised with that of the laser and the galvo mirror. The result is are three lists, where the first list contains the starting times of the laser pulse, the second list contains the starting times of the oscillation of the galvo mirror and the last list contains the times a photon was detected. From these we can reconstruct the emission intensity profiles as a function of the time after the laser pulse. b) A schematic overview of how rotating the galvo mirror can scan the emission profile. The light emitted from a position on the sample, falls on the lens and is collimated with an angle θ_{out} which depends on the position from where it emits. Because of this different angle, we can rotate the galvo mirror to tune which beam is directed to the centre of the other lens, which than focuses the light beam on the APD. c) The relationship between the position x and the voltage of the galvo mirror, we see that the relationship between these can indeed be approximated using a linear relationship. We find a conversion factor of $\alpha = 0.30$ µm mV^{-1}.

4 Results

4.1 Simulations

In this section, we show the results of the MC simulations to study the diffusion coefficient as an effect of the energy transfer from one ion to another. For this we compare the mean-field approach to a Monte-Carlo simulation. In figure 8d we show the mean-squared displacement as a function of time at an ion doping of 20% (yellow). We see that there are two regimes, at short timescales a fast diffusion and a slow diffusion at long timescales. We see that the fast-diffusive regime can indeed be described using a mean-field theory (red).

At longer timescales, however, we see that the slope of the mean-squared displacement has decreased and there is thus a smaller diffusion coefficient. This can be explained using figure 8c, where we show the return probability as a function of the ion-doping concentration for the mean-field theory (red) and the simulation (blue). The return probability we define as the probability that an excitation migrates backwards and forwards in two subsequent migrations. This probability is in the simulation always larger than in the mean-field theory. This can be explained using the knowledge where an excitation came from. For the first migration we know nothing about the environment of the site and each neighbouring site has an equal probability of being a donor. For the second migration, however, we know where the excitation came from, so we also know that that particular position is now a donor and therefore the probability of being a donor is slightly smaller for all other neighbouring sites. This results in a higher probability to migrate in exactly the opposite direction.

This long-time behaviour is quantified using a linear fit (blue) from which we can extract the diffusion coefficient using equation 2.6. In figure 8e we show the diffusion coefficients as a function of the ion-doping concentration for both the short- (red) and long-time (blue) regime. We see that the long-term diffusion coefficient is always smaller than the mean-field approach, as expected by the explanation above. We also see that in the limit that the ion doping approaches 100% the difference between the two regimes disappears. This is expected, since in this limit the neighbourhoods of all particles look the same, meaning that the mean-field approach is exact.

Lastly we studied the diffusion coefficient as function of the excitation doping (figure 8) for an ion doping concentration of 20% (light blue) and 90% (purple), which we expected to be linear as described in equation 2.9 and we see that this is indeed the case. This means that the diffusive behaviour does not change upon changing the excitation density.

Anisotropic Analysis We will also study the diffusion along the different unit cell vectors $\boldsymbol{a}$,$\boldsymbol{b}$ and $\boldsymbol{c}$. We note that $\boldsymbol{a}$ and $\boldsymbol{b}$ are in fact the same, which can be seen by rotation around the $\boldsymbol{c}$-axis. Comparing the $\boldsymbol{a}$- and $\boldsymbol{b}$-axis with the $\boldsymbol{c}$-axis we see that the nearest neighbour in the $\boldsymbol{c}$-direction is approximately half as near as in the other directions, meaning that migrations in that direction are more likely to happen. We would naively expect that the diffusion along the $\boldsymbol{c}$-axis is faster than in the other directions.

In figure 9a we show the diffusion coefficient as function of the ion doping along the $\boldsymbol{a}$- and $\boldsymbol{b}$- (orange) and $\boldsymbol{c}$-axis (purple). The first thing we note is that the diffusion coefficients have again the same behaviour as in the isotropic analysis, that is an overall smaller diffusion coefficient than the mean field approach up until a fully doped system, where both approaches give again the same values. Furthermore, we see that there are in fact two regimes, at low concentrations we have in fact an isotropic behaviour and at high concentrations we have we have indeed an anisotropic behaviour. This anistropic behaviour is expected, as we explained above.

To understand why there is such a transition, we took a closer look at the migration distance distribution for two migrations for both a low (20%) and a high (90%) concentration, as given in figure 9. In this we look at the return probability, defined as the probability that an excitation is back in the same plane as it started in. If these probabilities are about equal for the different directions, this would mean that the diffusion is equally likely in both directions, if the probabilities are not equal, there is a higher probability that it diffuses away in one of the two directions. This qualitatively explains the isotropic behaviour in the case of 20% doping, where the probabilities to move in either of the two direction are approximately equal, and the anisotropic behaviour in the case of 90% doping, where there is a much clearer difference between the two directions.

This is also shown in figure 9c, where we plot the return probability as a function of the ion doping concentration. This can be related to the probability to migrate away in that direction as $1 - P_i(0)$, where $P_i(0)$ is the return probability in direction i. From this we see that at low concentrations both return probabilities

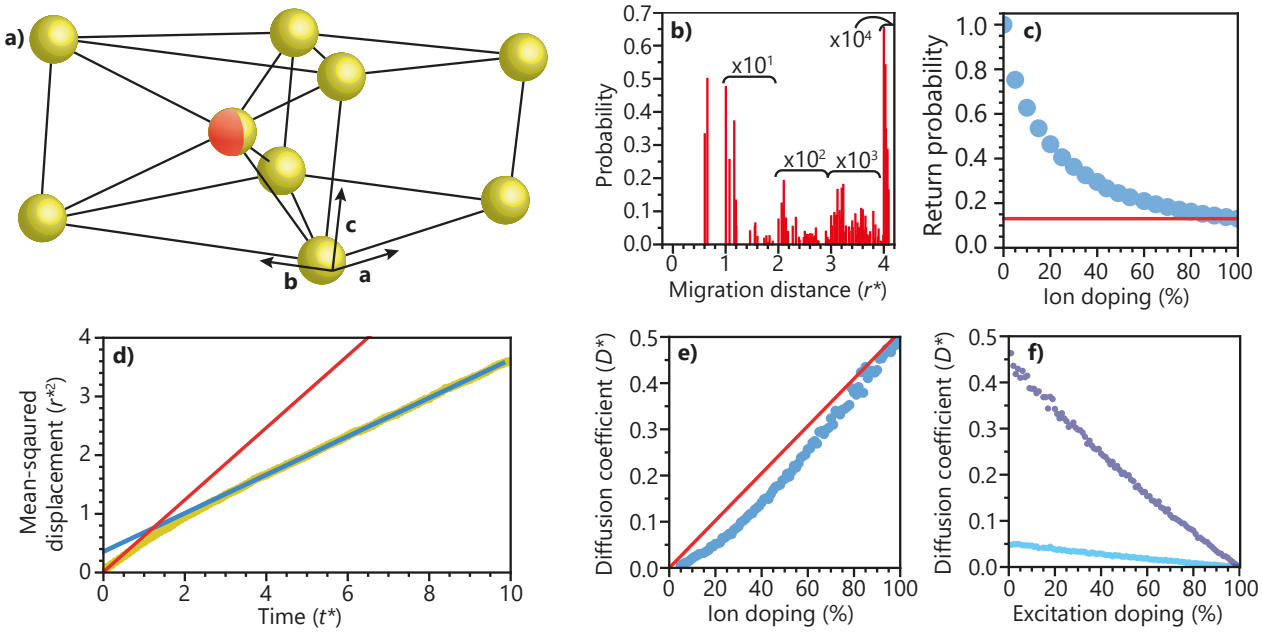

Figure 8: (a) A schematic overview of the yttrium positions in a β-$NaYF_4$ unit cell. The two coloured position is 50% occupied with an yttrium ion. The two positions are at $(0, 0, 0)$ and $(1/3, 2/3, 1/2)$, the angle between $\boldsymbol{a}$ and $\boldsymbol{b}$ is 120° and the unit cell parameters are $a = b = 5.96606(13)$Å and $c = 3.51738(6)$Å [9]. (b) The probability to find an excitation at a distance r^* away after a single migration. We see that the probability approximately decreases with a factor 10^{r^*} and it thus seems a fair approximation to set the cut-off radius (maximum distance an excitation can migrate in a single step) to about 4. (c) The probability that an excitation returns to the same position as it was one migration ago for the simulation (blue) and the mean-field theory. From this figure we see that the mean-field theory does not take into account the knowledge where an excitation has been. In fact there is a higher probability to move back, since we know that site is doped, which also means that all other sites are less likely to be doped. (d) The mean squared displacement of the migration of the excitations over the dopants in a 20% doped $NaYF_4$:Yb^{3+} crystal (yellow). We see that there are two regimes, at very short timescales we have a fast diffusion (red) and at longer timescales we have a slower diffusion (blue). The fast diffusion regime follows a mean-field model and the slow diffusion regime. We quantify the slow diffusion with a linear fit (blue) after $t^* = 3.5$. (e) The diffusion coefficient as a function of the ion doping for the fast mean-field diffusion in red and slow fitted diffusion in green. We see that the mean-field model overestimates the diffusion coefficient for low concentrations, while at high concentrations they give approximately the same value as expected since the mean-field theory is exact for a doping concentration of 100%. (f) The diffusion coefficient as a function of the excitation doping with an ion concentration of 20% (light blue) and 90% (purple). We observe a linear relation between them, which corresponds with the mean-field theory.

are approximately the same, indicating that the diffusion is isotropic. We also see that at high concentrations the return probability is smaller in the $\boldsymbol{c}$-direction, indicating that there is more diffusion along that axis, which is exactly what we observe.

As we look back to figure 8b, we note that the majority of the migrations are within the first two unit cells, which means that the transition point is probably some kind of perculation point below which there is no connected path of nearer neighbours and above which there is a connected path of nearer neighbours. This means that below the transition point the direction of the diffusion is limited by the neighbours farther away, which are more isotropic, and above the transition point the direction of the diffusion is limited by the nearer neighbours, which have these anisotropic distribution.

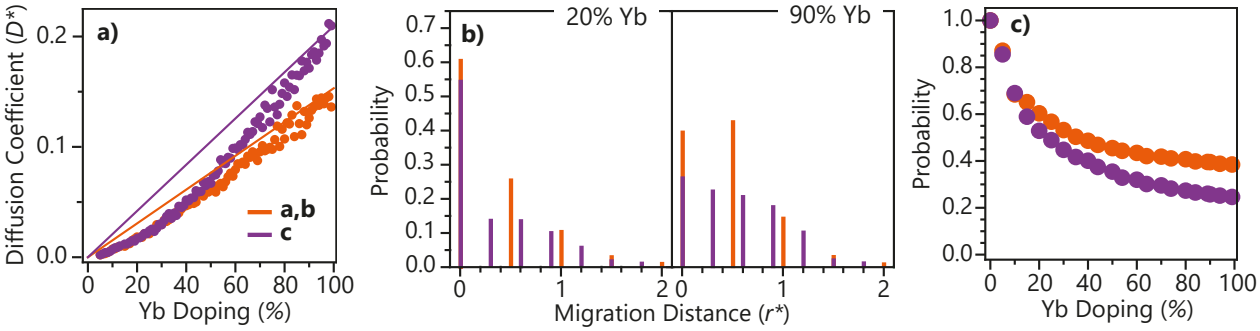

Figure 9: Comparison of the diffusion along the different directions in the unit cell $\boldsymbol{a}$, $\boldsymbol{b}$ (orange) and $\boldsymbol{c}$ (purple). (a) The diffusion coefficient for all different directions, where the solid line indicates the mean-field diffusion (short-term behaviour) and the dots the simulated diffusion (long-term behaviour). We see that the diffusion coefficients are the same up until about 35% and from there they increase approximately linear towards the mean-field value. (b) The migration distance distributions for two migrations at 20 and 90% ion doping concentrations. Here we primarily look at the probability for the excitation to end up in the same plane as it was two migrations ago. We note that there is a larger difference between the directions at high doping concentrations and they are approximately the same at low concentrations. This we also summarized in (c), where we plot the probability to end in the same plane as a function of the doping concentration. We see from these figures that the system has an isotropic diffusive behaviour at low concentrations and an anistropic behaviour at high concentrations.

4.2 Ytterbium doped nanocrystals

In this section we will look at the broadening of the emission intensities in a two level system, for which we used a sample that only contains Yb-ions as dopants. As we saw in the introduction, namely, we can describe an Yb-ion as a two energy level diagram as given in figure 10a, where we changed the names of the excitation parameters a bit. This means that we can use the theory from 2.3. In this section we derived two primary results:

1. We found for the steady state a relation between the excitation power and the width of the emission-intensity in the case of no diffusion, which we can write as

$$\gamma'^2 = \left(1 + \frac{C_{\mathrm{ex,Yb}} P}{k_{\mathrm{Yb}}}\right) \gamma^2, \tag{4.1}$$

   for a Lorentzian-shaped excitation-intensity.

2. We also found in the case that there is no excitation, that we can write the population in the excited state as the convolution between an initial profile and a Gaussian distribution with a width of $\sigma^2 = 2dD_{\mathrm{Yb}}t$

$$N_1(\vec{r}, t) = \frac{e^{-k_{\mathrm{Yb}}t}}{(4\pi d D_{\mathrm{Yb}} t)^{\frac{d}{2}}} \int_{-\infty}^{\infty} N_1\left(\vec{R}, 0\right) e^{-\frac{(\vec{r}-\vec{R})^2}{4dD_{\mathrm{Yb}}t}} \mathrm{d}\vec{R}. \tag{4.2}$$

   This equation reduces to

$$N_1(\vec{r}, t) = e^{-k_{\mathrm{Yb}}t} N_1(\vec{r}, 0) \tag{4.3}$$

   in the limit that the diffusion goes to zero.

Since the first relation is based on the assumption that there is no diffusion, we first look at the results of time-dependant measurements, as given in figures 10b and c. In these measurements the excitation time is 1ms. In 10b we show the total intensity as a function of time at different excitation powers, where we see that the decay is the same for all curves apart from the very end, where the curves flatten. This is due to noise and depends on the signal to noise ratio and the number of the measurements.
The equal decay behaviour is expected, since the decay only depends on the number of excited states. Since diffusion does not change this number, the decay rate does not change either. This can also be seen by integrating equation 4.2 over the whole area, which yields $I_1(t) = I_1(0)e^{-k_{\mathrm{Yb}}t}$, where $I_1(t) = \int N_1(\vec{r}, t)\, dA$. And fitting $\frac{I_1(t)}{I_1(0)} = e^{-k_{\mathrm{Yb}}t} + c$ gives a decay parameter $k_{\mathrm{Yb}} = 2.65 \pm 0.03\mathrm{ms}^{-1}$.
In order to see if there is any diffusion at all, we look at the width of the emission intensity as a function of time, which is given in figure 10c. Here we define the width as the γ-parameter in a Lorentzian fit $\left(1 + \left(\frac{x}{\gamma}\right)^2\right)^{-1}$. In this figure we see that the width stays the same after the excitation source is turned off, which is the prerequisite for statement 2. This indicates that there is no diffusion of excited states in this sample. Since the number of Yb-ions in the NCs is approximately a factor 9 larger than the number of Er-ions, it is only a fair estimate that there is also no diffusion of energy over the Er-ions. Which means that it is probably a fair approximation to neglect any diffusion further on.
On the other side, we see that there is a broadening effect during the excitation, which can be explained using equation 4.1. Here we see that the steady state emission profile is broader than the excitation profile, which means that during the excitation there is broadening. At the very beginning, when the laser is just turned on, the emission profile has exactly the same width as the excitation profile, since the excited state populates linearly at these time scales. So when the laser is on, the width increases from the initial width, which is equal to the excitation intensity width, to the steady-state width as given in equation 4.1. This steady-state emission width increases as the excitation power increases, which means that there is more broadening during the excitation phase. This is exactly what we observe.
In figure 10d we show the steady-state emission intensity profile at an excitation power of 6.6mW as seen on the camera, where green indicates a low intensity and red indicates a high intensity. From this figure we see that the emission intensity is radially symmetric. And in figure 10e we show a slice through this intensity

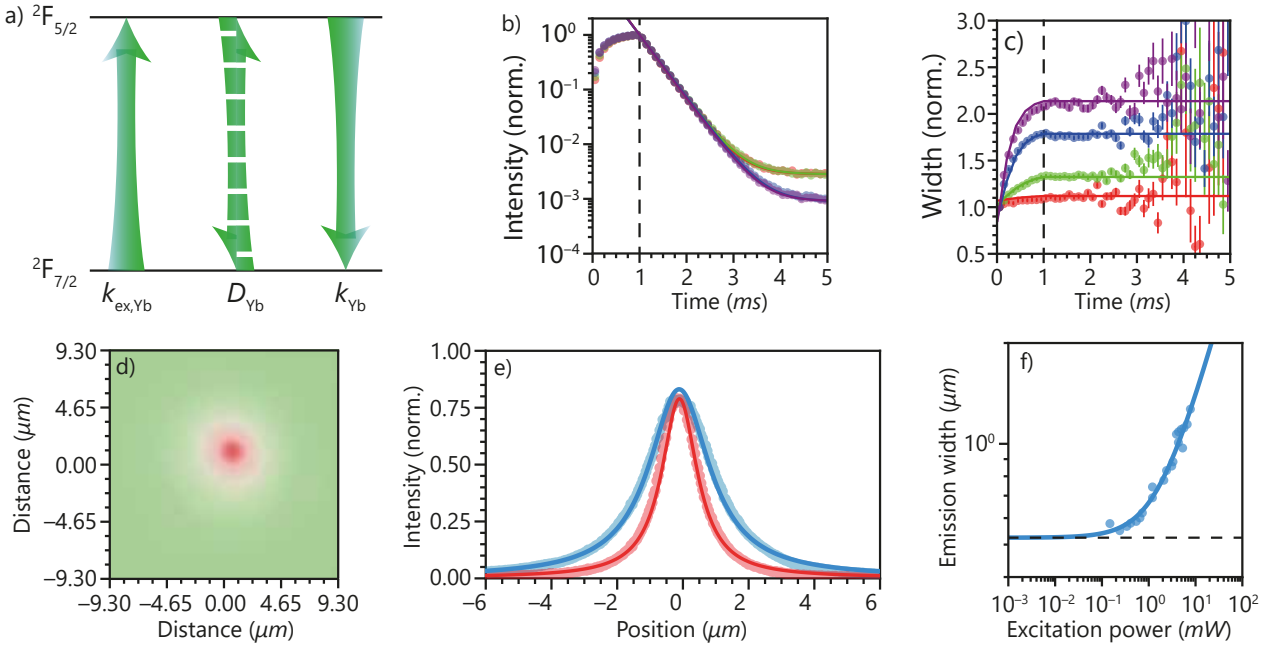

Figure 10: a) The simplified energy-level diagram for the ytterbium ions, where the energy difference corresponds to 980nm infra-red light. This diagram is the same as the one we used in section 2.3, such that we can use those results. b) The emission-intensity as a function of time with an excitation power of 0.2mW (red), 1.3mW (green), 5.6mW (blue) and 10.2mW (purple) and an excitation time of 1ms. The intensity is normalised, such that the maximum intensity, which is at $t = 1$ms, equals 1. The solid lines are fits of a decay behaviour from which we obtain $k_{\mathrm{Yb}} = 2.65 \pm 0.03\mathrm{ms}^{-1}$. We see there is a small difference in excitation part, which is a result a faster excitation. On the other side we see that there is a plateau of the decay curves, which is due to the noise of the measurement. c) The width of the emission-intensity profile with the same conditions as in b). We define the width as the γ-parameter of the Lorentzian fit. We see that the width increases in time while the laser is turned and this effect increases as the power increases, as we expect from equation 4.1. When the laser is off, we no longer see the width changing, which means that there is no diffusion of the excited states. In the end we see that error-bars become very large, which is due to the very low signal to noise ratio. d) A camera intensity distribution of a steady-state shot with an excitation power of 6.6mW. From this picture we see that the intensity profile has radial symmetry. This means that we can indeed use the 2d Lorentzian function, where the x is simply replaced by $\vec{r}$. e) A one-dimensional slice through the measured emission intensity profiles at an excitation power of 0.7 mW in red and 6.6 mW in blue. In this figure the solid lines are Lorentzian fits to the 2d distributions as shown in d). We see that the Lorentzian fit quite accurately describes the width of the profile. In the centre, however, we see that the fit overestimates the data, which is due to a small Gaussian component in the excitation profile. This component broadens less and broadens its top, as we saw in section 2.3, which gives the flattened top. f) The measured emission peak widths as a function of the excitation power, where the dots indicate the data and the line is a fit of the Lorentzian width model described in equation 4.1. We see that this model agrees with the data, and we find the parameters $\gamma = 520 \pm 20$ nm and $\frac{C_{\mathrm{ex,Yb}}}{k_{\mathrm{Yb}}} = 0.62 \pm 0.07\ \mathrm{mW}^{-1}$, which translates with the value of k_{Yb} to an absorption cross-section $\sigma_{\mathrm{ex,Yb}} = (5.6 \pm 0.6)\, 10^{-20}\mathrm{cm}^2$

profile at 0.7 and 6.6mW together with Lorentzian fits. We see that this fit quite accurately describes the shape and thus width of this profile. From these two figures, we can conclude that our approximation of the excitation-intensity profile as a radially-symmetric Lorentzian is quite accurate. And we can thus use these fits as indication of the width of these profiles.
The widths of Lorentzian fits through the steady-state intensity profiles are shown in figure 4f as a function of the excitation power. Through this data we fitted our expected model as given in equation 4.1. Here we see that the data follows the model almost exactly. This model fit gives us an excitation power density width of 520 ± 20 nm and $\frac{C_{\mathrm{ex,Yb}}}{k} = 0.62 \pm 0.07$ mW^{-1}. This can be converted to the ratio $\frac{\sigma}{k} = 2.0 \pm 0.2 \cdot 10^{-20}$ ms cm^2. Here we used that the excitation source has a wavelength of 980 nm and we approximated the integral with a numerical integration of the the emission profile at 0.24 mW, which has approximately the same shape and width as the excitation power density profile. Combining this with the decay-parameter k_{Yb} we found earlier, we find $\sigma_{\mathrm{ex,Yb}} = (5.6 \pm 0.6)\, 10^{-20}\mathrm{cm}^2$ and $k_{\mathrm{Yb}} = 2.65 \pm 0.03\mathrm{ms}^{-1}$.
With these values, we calculated the time-dependant width as a function of time using the differential equation for a two-level system where we use the parameters we found. These results are shown in figure 10c and we see that this theory indeed matches with the measurement.

4.3 Erbium doped nanocrystals

In this section, we look at the results of the broadening and narrowing effect of the emission intensity in three level systems. For this we first summarize the analytical results we found in section 2.4, where we calculated some limits for a three-level system where the energy spacing between the ground state and the first excited state equals the energy spacing between the first excited state and the second excited state. These results can be summarized as

1. If the upconversion rate is much faster than the cross-relaxation rate $k_{\mathrm{UC}}N_1^2 >> k_{\mathrm{CR}}N_0N_2$, the width γ of the emission profile increases as

$$\frac{\gamma(t)^2}{\gamma(0)^2} = 1 + A_1c_1 - A_1c_1e^{-k_1t} \tag{4.4}$$

   where $c_1 = \frac{2k_{\mathrm{UC}}}{k_1}$ and A_1 is the amplitude of the initial emission profile in state 1.

2. If the upconversion rate is much slower than the cross-relaxation rate $k_{\mathrm{UC}}N_1^2 << k_{\mathrm{CR}}N_0N_2$, the width γ of the emission profile decreases as

$$\frac{\gamma(t)^2}{\gamma(0)^2} = 1 + A_2c_2 - A_2c_2e^{-kt} \tag{4.5}$$

   where $k = k_{\mathrm{CR}} + k_2$ and $c_2 = \frac{k_{\mathrm{CR}}}{k}$ is the amplitude of the initial emission profile in state 2.

3. If the excitation is very short we can write these amplitudes as

$$A_{\mathrm{i}} = \frac{\lambda\sigma_{0\mathrm{i}}t_{\mathrm{pulse}}}{hc\int_{\mathrm{dA}} f(\vec{r})\mathrm{dA}}P \tag{4.6}$$

   where λ is the wavelength of the excitation source, $\sigma_{0\mathrm{i}}$ is the absorption cross-section for the excitation from the ground state to state i, t_{pulse} is the duration of the excitation pulse, P is the excitation power, h and c are respectively Planck's constant and the speed of light (in vacuum), $f(\vec{r})$ is the laser profile normalized, such that the maximum is 1.

In this section we compare these analytical limits with experiments and try to replicate the behaviour using found parameters. For this we use a three level representation of the Er- and Yb-ions as seen in the introduction. This representation is given in figure 11a. Note that we do not make a difference between the different ion species, but consider them as if they are one. This means, however, that the parameters that we find will be effective parameters and only be valid for this specific sample, since they depend on the ratio of the different species and the ion density.
In figure 11b we show the width of the emission intensity as a function of time for an IR excitation and IR emission for $NaY_{0.8}F_4$:$Er_{0.02}{}^{3+}Yb_{0.18}{}^{3+}$-NCs. These measurements are taken with a excitation time of $t_{\mathrm{pulse}} = 0.1$ms at powers in the range of $0.1 - 1.2$mW, such that we are in the limit of low powers and short excitation. These measurements correspond to the first limit, where the upconversion rate is much faster than the cross-relaxation rate, so the width should follow equation 4.4. We normalized the width, such that the width at $t = t_{\mathrm{pulse}}$ equals one, such that it corresponds with the equation. The colours indicate from red to purple an increasing power and the lines are fits to the data in the regime $t_{\mathrm{pulse}} < t < t_{\mathrm{max}}$, where t_{max} is the time that corresponds to the maximum width. In order to obtain the upconversion rate constant, we assumed that the absorption cross-section $\sigma_{01} = \sigma_{\mathrm{Yb}}$. This assumption is based on the fact that 90% of the excitable ions is an Yb-ion. The two rate constants k_1 and k_{UC} that were obtained by the fits are given in table 1. In these values, we see that there is a error for the found values, which is due to the fact that there are only a few points to fit through, since the equation does not describe the entire behaviour.
In this figure we see that the broadening effect indeed increases as the power increases, as we would expect from filling in equation 4.6 in equation 4.4. We also see, however, that the width does not increase to a maximum width and then stays there, as we would expect from just looking at the limiting behaviour, but the width decreases again. This can be explained using the fact that this limit is only true at short timescales. At long timescales, however, the population in the first excited state is depleted, while the population in the

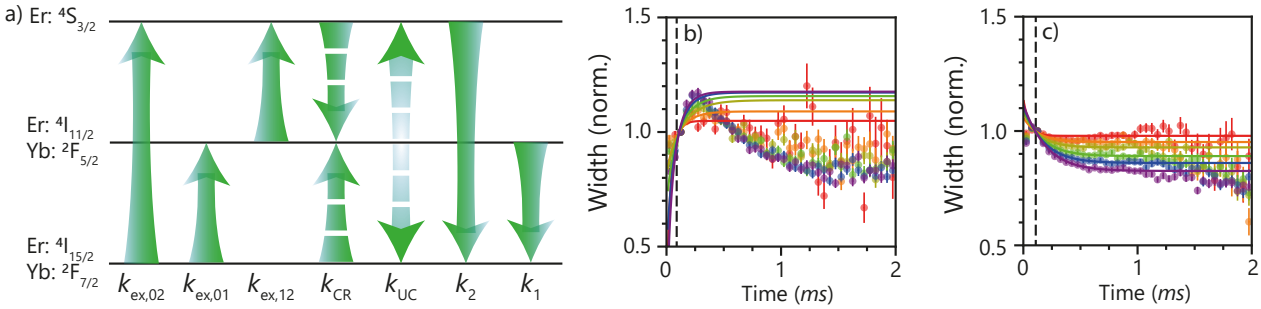

Figure 11: a) The energy level scheme that we consider for these experiments, in which we only changed the names of the energy states. Note, however, that we do not consider the fact that there are different ion species, where the Yb-ions have one excited state and the Er-ions have two excited states. This means that the parameters involving the second energy level are in fact effective parameters, which depend on the on the ratio of the different species. b) The emission width of the IR level with an IR excitation as a function of time for $NaY_{0.8}F_4$:$Er_{0.02}{}^{3+}Yb_{0.18}{}^{3+}$-NCs. The colours indicate the different powers 0.1 mW (red), 0.3 mW (orange), 0.5 mW (yellow), 0.7 mW (green), 1.0 mW (blue) and 1.2 mW (purple). The excitation duration $t_{\text{pulse}} = 0.1$ ms and the width is normalized, such that it is one at $t = t_{\text{pulse}}$. We see that first the emission intensity profile broadens, which is due to the fast upconversion, and then narrows, which is due to the delayed cross-relaxation. c) The emission width of the green level with an green excitation as a function of time for $NaY_{0.98}F_4$:$Er_{0.02}{}^{3+}$-NCs. The colours indicate the different powers 0.2 mW (red), 0.3 mW (orange), 0.5 mW (yellow), 0.7 mW (green), 1.0 mW (blue) and 1.2 mW (purple). The excitation duration $t_{\text{pulse}} = 0.1$ ms and the width is normalized, such that it is one at $t = t_{\text{pulse}}$. In this case there is only a narrowing of the emission intensity profile, which is due to the fact that the effective decay of the first excited state is much faster than the effective decay of the second excited state. The parameters found using the fits in b) and c) are given in table 1.

second excited state has increased, such that the cross-relaxation process is now the most important process, which means that there is an effective feeding process with a narrower profile, which leads to a narrowing of the first excited state emission profile.

In figure 11c, we show the width of the emission intensity as a function of time for an green excitation and green emission for $NaY_{0.98}F_4$:$Er_{0.02}{}^{3+}$-NCs. These measurements are taken with a excitation time of $t_{\text{pulse}} = 0.1$ms at powers in the range of $0.1 - 1.2$mW, such that we are in the limit of low powers and short excitation. These measurements correspond to the second limit, where the upconversion rate is much slower than the cross-relaxation rate, such that the width should follow equation 4.5. We normalized the width, such that the width at $t = t_{\text{pulse}}$ equals one. The colours indicate from red to purple an increasing power and the lines are fits to the data after $t = t_{\text{pulse}}$. We see that the narrowing effect increases as the power increases, which is exactly as we would expect from equation 4.5.

In this figure, we also see that there in not an increase in width after a certain time. So in this regime, there is no effective filling of the first excited state as the second excited state depletes, this can be explained by the average lifetime as we summarized in table 1. In this table, we see that the second excited state lives longer than the first excited state, so there is no population build-up in the first excited state. The first excited state decays faster than it grows.

In figure 12 we compare the experiments with numerical solutions of the full differential equations. In 12a) we see that the differential equations follow the data quite well with the parameters as we found them. This could be a bit surprising, since the value for the upconversion rate was obtained in an experiment, where there sample contained Yb, in contrast with this sample, which does not contain it. We would expect that the needed upconversion parameter is much smaller, so apparently the upconversion parameter is not that important, since the decay of the first excited state is fast enough that there is no feedback on the green energy level.

In figure 12b) we compare the data at the highest power with the solution to the differential equation with the parameters as given in table 1, which is represented by the dotted line. We see that this line does not align with the data whatsoever. However, it approximately gives the correct overall behaviour, first the

Parameters	Value	Units	Comments
σ_{Yb}	$(5.6 \pm 0.6) \cdot 10^{-20}$	cm^2	From the previous section
σ_{02}	$(2.1 \pm 0.3) \cdot 10^{-19}$	cm^2	
σ_{01}	$(5.6 \pm 0.6) \cdot 10^{-20}$	cm^2	Taken to be equal to σ_{Yb}
σ_{12}	0	cm^2	Assumption
k_{Yb}	2.65 ± 0.03	ms^{-1}	From the previous section
k_1	10 ± 4	ms^{-1}	
k_2	2.2	ms^{-1}	From paper[9]
k_{CR}	(4.4 ± 0.6)	ms^{-1}	
k_{UC}	(6 ± 3)	ms^{-1}	

Table 1: The rate constants as found from the experiments with low-power and short excitation time.

width increases and then it decreases again. With this in mind, we fiddle around with the very uncertain parameters within their 99%-confidence interval to obtain the solid lines. We see that these solutions describe the behaviour of the data quite accurately.
So now that we have found a solution that can describe the behaviour of these short-excitation, low-power experiments, we can try to match them to measurements with a longer excitation duration as given in figure 12. In this experiment, we excite using an IR laser and look at the resulting IR (red) and green (green) emissions, where the bright colours indicate a higher power and the dark colours indicate a lower power. The lines are for the higher power solution and we see that the IR solution matches the data up until the laser is turned off, the green line, however does not follow the data at all. This can be an effect that we assumed the absorption cross-section $\sigma_{12} = 0$. In the previous section, we saw that non-linear saturation effects lead to a broadening of the emission peak during the laser pulse. The broadening we see now, however, is solely due to the broadening of the IR level, which broadens the green level as well due to a broader feeding of this level. These non-linear saturation effects of the green level, would also explain the difference in broadening between a high and a low power. As we saw earlier, a higher power broadens more than a low power.
After the laser pulse is turned off, we see that for the solutions to the differential equations the width of the emission intensity immediately decreases. This means that the second excited state would have been sufficiently filled to counteract the broadening due to the upconversion. In the data, however, we see that this is clearly not the case. This could either be a hint that, although we have not seen it directly, there is some diffusive behaviour or this could be the effect of a delayed upconversion process of two excited Yb-ions. We can think of it like this, when we excite the system in the IR, there can be two separate upconversion processes, the first one being the direct one, where one Er-ion in the first excited state combines with a either another Er-ion in the first excited state or with an excited Yb-ion, or the other process, where two excited Yb-ions combine. In this second process, there is an intermediate step, where one of the excited Yb-ion transfers its energy to an Er-ion in the ground state. This thus means that we have an more or less 'instant' process and a delayed process. This delayed process could then increase the broadening effect at long excitation times, since the Yb-ions are filled, which leads to a higher effective upconversion rate, which leads to a longer broadening effect as can be seen from equation 4.4.
Something else to note here, is that we only consider three possible states for the Er-ions, while in fact there are many more. This also means that there are many more pathways to the green level and the importance of the different pathways change as the excitation conditions change. Using higher powers, for example decreases the relative population of the green level with respect to the red level[9], which lies somewhere between our first and second excited state. These different pathways could also have some effect on the emission widths and it might be a good idea to include these other levels in future research.

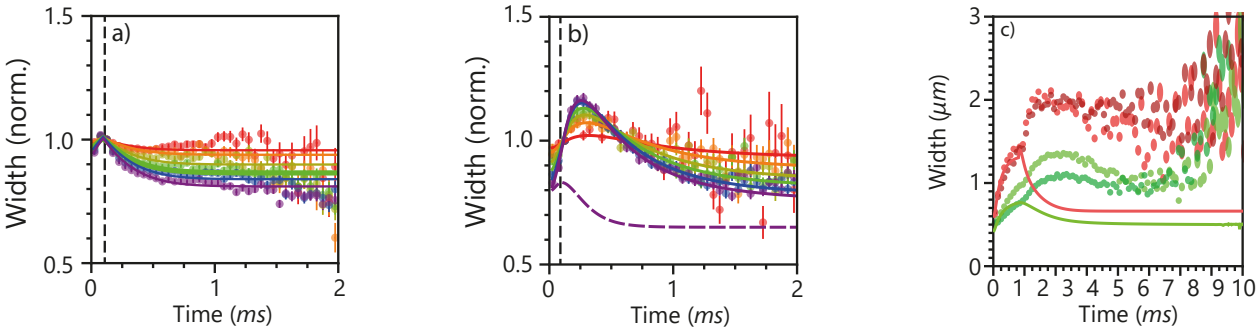

Figure 12: a) The same measurements as in figure 11c, but the solid lines now indicate a numerical solution of the original differential equations as given in section 2.4, where we used the parameters as given in table 1 and only changing the initial width. We see that the differential solution matches pretty well with the experiments, although we would not expect that the upconversion constant is the same, since this sample does not contain Yb. This can be explained with the fact that the decay of the first excited state is very fast, such that there is little to no effect of this parameter. b) The same measurements as figure 11b, where the dotted line indicates a numerical solution of the original differential equations as given in section 2.4 with the parameters as given in table 1. The solid lines are made when changing the parameters $k_1 = (10 \pm 4)\text{ms}^{-1}$ and $k_{\text{UC}} = (6 \pm 3)\text{ms}^{-1}$ to $k_1 = 3.3\text{ms}^{-1}$ and $k_{\text{UC}} = 12\text{ms}^{-1}$. We see that we heavily improved the correspondence to the data by changing these parameters. c) The width of the emission intensity profile as a function of time on $NaY_{0.8}F_4$:$Er_{0.02}{}^{3+}Yb_{0.18}{}^{3+}$-NCs. In these experiments, we used an IR excitation source with an excitation power of 0.2 mW (light dots) and 0.7 mW (dark dots) for 1ms. The green dots indicate the green emission of the second excited state and the red dots indicate the IR emission of the first excited state. The lines are solutions to the differential equations, with the parameters that gave a matching behaviour in b). We see that, although, the differential equations were able to match one experiment, they are not able to predict this experiment.

5 Conclusions

In this thesis, we first showed the relation between the diffusion of energy over dopants in a $NaYF_4$ crystal and the doping concentration. This relation has some kind of perculation point below which the diffusion coefficient is isotropic and increases slower and above which the diffusion coefficent increases faster with respect to the doping concentration and diffuses faster in one the directions. After we found this relation, we analyzed the emission intensity profiles for $NaYF_4$ NCs doped with Yb and/or Er. In these measurements, we showed that for Lorentzian-distributed excitation intensities the excitation saturation and the upconversion process lead to a broadening of the emission profile, while the cross relaxation leads to a narrowing of the emission intensity profile. By tuning the found parameters a bit within their margin of error, we were able to match the solution to the differential equation to the measurements at low power. When we compared the numerical solutions to the measurements at high power, however, we saw that the numerical solution was not even close.

Overall, we showed that this method of measuring the intensity profile can give us insights into the different processes that play a part in these upconversion materials. This means that it can play a role in constructing a more complete energy level diagram and they should definitely be considered as another method to check or fit the model to. An issue that needs to be solved, however, is the exact excitation intensity profile. This cannot be a true Lorentzian as we used, since that would mean that the total power is infinite.

To improve the model, one could consider separating the Yb and Er to form a coupled energy diagram, another improvement would be the addition of two extra energy levels, such that there are two separate CR and UC processes, one where the energy is back transferred to the ytterbium ion and the other, which involves the two extra levels. Another possible improvement is the addition of an energy level that lies above the green level, such that the Er can effectively absorb three photons. These new energy levels lead to different pathways to emission, which play different roles at different powers.

Something else one could consider doing, is to change the excitation profile, to for example a more Gaussian shape. As we showed in section 2.3, the broadening due to excitation saturation broadens a Gaussian excitation profile much less than a Lorentzian one. This means that the broadening due to diffusion, which does not depend on the profile, is relatively larger for a profile with steeper tails.

Finally one could improve the MC simulations bye for example adding the nanocrystal structure of the system to see how this interparticle diffusion is related to the intraparticle diffusion. Another path of exploration could be the addition of explicitly using two different dopants with different interaction strengths, thus also different energy transfer rates.

References

[1] Martin Kaiser et al. 'Explaining the influence of dopant concentration and excitation power density on the luminescence and brightness of β-NaYF4:Yb3+,Er3+ nanoparticles: Measurements and simulations'. In: *Nano Research* 12.8 (Aug. 2019), pp. 1871–1879. ISSN: 1998-0124. DOI: 10.1007/s12274-019-2450-4. URL: http://link.springer.com/10.1007/s12274-019-2450-4.

[2] Freddy T. Rabouw et al. 'Quenching Pathways in NaYF4:Er3+,Yb3+ Upconversion Nanocrystals'. In: *ACS Nano* 12.5 (2018), pp. 4812–4823. ISSN: 1936086X. DOI: 10.1021/acsnano.8b01545.

[3] John-Christopher Boyer. 'Synthesis and Spectroscopy of Upconverting lanthanide-Doped Nanocrystals'. In: December (2006).

[4] Robin G. Geitenbeek et al. 'Nanocrystals for Luminescence Thermometry up to 900'. In: *Journal of Physical Chemistry C* 121.6 (2017), pp. 3503–3510. ISSN: 19327455. DOI: 10.1021/acs.jpcc.6b10279.

[5] Xingwen Cheng et al. 'Er3+ Sensitized Photon Upconversion Nanocrystals'. In: *Advanced Functional Materials* 28.22 (2018), pp. 1–6. ISSN: 16163028. DOI: 10.1002/adfm.201800208.

[6] Markus Haase and Helmut Schäfer. 'Upconverting nanoparticles'. In: *Angewandte Chemie - International Edition* 50.26 (2011), pp. 5808–5829. ISSN: 15213773. DOI: 10.1002/anie.201005159.

[7] Guokui Liu. 'Advances in the theoretical understanding of photon upconversion in rare-earth activated nanophosphors'. In: *Chemical Society Reviews* 44.6 (2015), pp. 1635–1652. ISSN: 14604744. DOI: 10.1039/c4cs00187g.

[8] Zijun Wang and Andries Meijerink. 'Concentration Quenching in Upconversion Nanocrystals'. In: *Journal of Physical Chemistry C* 122.45 (2018), pp. 26298–26306. ISSN: 19327455. DOI: 10.1021/acs.jpcc.8b09371.

[9] Pedro Villanueva-Delgado, Karl W. Krämer and Rafael Valiente. 'Simulating Energy Transfer and Upconversion in β-NaYF4: Yb3+, Tm3+'. In: *Journal of Physical Chemistry C* 119.41 (2015), pp. 23648–23657. ISSN: 19327455. DOI: 10.1021/acs.jpcc.5b06770.

[10] Theodor Főrster. 'Delocalized excitation and excitation transfer'. In: *U.S. At. Energy Comm. FIELD Full Journal Title:* FSU-2690-1.18 (1965), 61 pp.

[11] *DLMF: NIST Digital Library of Mathematical Functions*. http://dlmf.nist.gov/7.19, Release 1.1.4 of 2022-01-15. 2011. URL: http://dlmf.nist.gov/.